carbonate production of 100 mmol C m^{-2} day^{-1} (1.2 g C m^{-2} day^{-1}) in March 1993 (*12*). The ratio of organic production to calcium carbonate production is 1.1. The ratio was almost the same in August 1992 (1.0). The ratio of organic carbon production to calcium carbonate production required to maintain seawater P_{CO_2} at a constant value of 350 μatm has been calculated to be 0.6 (*2*). When the ratio exceeds these values, reefs serve as a sink of CO_2 (*13*). The ratio for Shiraho reef exceeds these threshold values, which is consistent with our P_{CO_2} measurements.

On Moorea barrier reef, French Polynesia, CO_2 evasion from sea to air was observed at a backreef site, and it was concluded that reefs are a source of CO_2 (*6*). In contrast, at a reef front (corresponding to the reef crest in this study) site, CO_2 flux from air to sea was observed (*14*). These results suggest that different reef zones act differently as to CO_2 fluxes and that the highly productive zone such as the reef front acts as a sink of CO_2.

A relatively low estimate of global reef net organic production was based on a mean reef production rate of 0.1 g C m^{-2} day^{-1} (*4*), which in turn was based primarily on measurements from three atolls (*15*). In that study, net production for the whole reef was calculated from changes in total carbon and alkalinity in enclosed lagoon water with a long residence time (50 days). Decomposition of organic matter predominated in such lagoons, and thus, the estimate might have been low. The low estimate of net organic production is also based on underestimates of the contribution of nitrogen fixation (*4*), which provides new nutrients for net organic production in the coral reef. Coral reefs, on the other hand, are known to be active sites of nitrogen fixation (*16*). Our P_{CO_2} measurements and our estimate of high net organic production indicate that reefs might serve as a sink, not a source, for atmospheric CO_2.

REFERENCES AND NOTES

1. S. V. Smith, *Nature* **273**, 225 (1978); J. D. Milliman, *Global Biogeochem. Cycles* **7**, 927 (1993).
2. J. R. Ware, S. V. Smith, M. L. Reaka-Kudla, *Coral Reefs* **11**, 127 (1992); M. Frankignoulle, C. Canon, J.-P. Gattuso, *Limnol. Oceanogr.* **39**, 458 (1994).
3. W. H. Berger, *Palaeogeogr. Palaeoclimatol. Palaeoecol.* **40**, 235 (1982); B. N. Opdyke and J. C. G. Walker, *Geology* **20**, 733 (1992).
4. C. J. Crossland, B. G. Hatcher, S. V. Smith, *Coral Reefs*, **10**, 55 (1991).
5. D. W. Kinsey and D. Hopley, *Palaeogeogr. Palaeoclimatol. Palaeoecol.* **89**, 363 (1991).
6. W. S. Broecker and T. Takahashi, *J. Geophys. Res.* **71**, 1575 (1966); J.-P. Gattuso, M. Pichon, B. Delesalle, M. Frankignoulle, *Mar. Ecol. Progr. Ser.* **96**, 259 (1993). Broecker and Takahashi measured spatial and temporal P_{CO_2} changes in water on the Bahama Banks and discussed the relation of those changes with calcium carbonate precipitation. Their site was on a shallow carbonate bank and not on a coral reef. Gattuso *et al.* measured the air-sea flux of CO_2 by monitoring the partial pressure of CO_2 in air inside a floating chamber on a barrier reef of Moorea, French Polynesia. This method did not monitor seawater P_{CO_2} directly.
7. H. Saito *et al.*, in press. We used a membrane instead of a spray as an equilibrator. Gaseous CO_2 diffuses through the membrane into flowing air inside the membrane tube, and its CO_2 concentration is measured by NDIR. P_{CO_2} changes in seawater were monitored continuously with the combined standard uncertainties of ±10 μatm in 1993 and ±5 μatm in 1994 estimated from NDIR calibration and vapor correction.
8. R. J. Planck, D. E. McAllister, A. T. McAllister, *Shiraho Coral Reef and the Proposed New Ishigaki Island Airport, Japan* (International Union for Conservation of Nature and Natural Resources, Switzerland, 1988).
9. The P_{CO_2} data are in situ values in microatmospheres (1 μatm = 0.101325 Pa). The study site is situated on a reef flat (mean depth of 200 cm) surrounded by coral patches. We set the P_{CO_2} measurement system 50 cm above the reef floor. The water was well mixed vertically by currents >2 cm s^{-1}. We measured the water temperature and salinity at the same time we measured P_{CO_2}. The maximum changes in temperature and salinity were 2°C and 0.1, and the estimated thermodynamical effects of these changes on P_{CO_2} at 350 μatm were 30 and 1.5 μatm [R. F. Weiss, R. A. Jahnke, C. D. Keeling, *Nature* **300**, 511 (1982)], respectively, except for the night from 13 to 14 March 1994 when the temperature changed 4°C. Therefore, the large P_{CO_2} change of more than 300 μatm was mainly the result of biological metabolism.
10. The global solar radiation was observed at Ishigaki Local Meteorological Observatory 5 km west of Shiraho reef. The mean light intensity (photosynthetically available radiation in micromoles per square meter per second) for March was calculated from the radiation records (megajoules per square meter) from 1986 to 1990 with the relation described by K. S. Baker and R. Frouin [*Limnol. Oceanogr.* **32**, 1370 (1987)] and A. Morel and R. C. Smith [*ibid.* **19**, 591 (1974)].
11. Estimation procedures were based on those of S. V. Smith [*ibid.* **18**, 106 (1973)] and are described by A. Suzuki [*Bull. Geol. Surv. Jpn.* **45**, 573 (1994)].
12. These production rates are within the range of the reported values in reefs [D. W. Kinsey, Proceedings of the Fifth International Coral Reef Congress, Tahiti, 27 May to 1 June 1985 (Antenne Museum-EPHE, Moorea, French Polynesia, 1985), vol. 4, p. 505. Shiraho reef is a typical tropical reef [J. E. N. Veron and P. R. Minchin, *Cont. Shelf Res.* **12**, 835 (1992)]; therefore, our results may be typical for fringing coral reefs with flourishing corals.
13. The coexistence of photosynthesis and calcification in reefs has been documented [H. Kayanne and S. Miyachi, *Biofutur* **106**, 76 (1991); T. A. McConnaughey, *Bull. Inst. Oceanogr. (Monaco)* **13**, 137 (1994); A. Suzuki, T. Nakamori, H. Kayanne, *Sediment. Geol.*, in press].
14. The large air-to-sea CO_2 flux at the reef front was interpreted as being due to the presence of recycled water from the reef. This interpretation, however, implies that the reef as a whole serves as a sink of CO_2.
15. S. V. Smith, *Natl. Oceanic Atmos. Adm. Symp. Ser. Undersea Res.* **1**, 127 (1983).
16. W. J. Wiebe, R. E. Johannes, K. L. Webb, *Science* **188**, 257 (1975); A. W. D. Larkum, I. R. Kennedy, W. J. Muller, *Mar. Biol.* **98**, 143 (1988); N. Shashar, T. Feldstein, Y. Cohen, Y. Loya, *Coral Reefs* **13**, 171 (1994); M. Yamamuro, M. Minagawa, H. Kayanne, Proceedings of the Seventh International Coral Reef Symposium, Guam, 22 to 27 June 1992 (Univ. of Guam Press, 1992), vol. 1, p. 358. *Limnol. Oceanogr.* **40**, 617 (1995).

17. We thank M. Yamamuro, K. Nozaki, C. Takahashi, I. Koike, and K. H. Cole for discussions during this study and the reviewers for their constructive comments. We also thank H. Hata, Y. Ikeda, M. Taira, and Fuyo Ocean Development and Engineering Company for their assistance in the field. Funding was provided by R&D for Global Environmental Technology of the Agency of Industrial Science and Technology, Ministry of International Trade and Industry, Japan.

27 October 1994; accepted 17 May 1995

Flotation of Diamond in Mantle Melt at High Pressure

Akio Suzuki, Eiji Ohtani, Takumi Kato

Experiments show that diamond floats in a primitive mantle melt at around 20 gigapascals and 2360°C and in a melt formed by partial melting of the transition zone at about 16 gigapascals and 2270°C. These observations constrain magma densities at high pressure. Diamond precipitated or trapped in a silicate melt at the base of the transition zone or the lower mantle floats and has been accumulating in the transition zone since early in Earth's history. Thus, the transition zone could be a reservoir of diamond.

Density difference between solid and liquid governs the chemical differentiation in the Earth's interior; in particular, the olivine-silicate melt density crossover at high pressure could produce serious influences (*1*, *2*). Density measurements at high pressure and high temperature have suggested that olivine floats in komatiite and peridotite melts at depths below 250 km (*3*, *4*). However, the existence of a density crossover between olivine and a magma in the Earth is still uncertain because flotation of olivine in the equilibrium mantle melt has not yet been observed in the experiments. Kitamura (*5*) suggested that diamond might float in mantle melt at high pressure and speculated that a diamond-rich layer might form during solidification of a terrestrial magma ocean.

We conducted density measurements of peridotite melts at high pressure by sink-float experiments with diamond as a density marker. The experiments were carried out in an MA-8–type multianvil apparatus (*6*). The starting materials (Table 1) were simplified compositions of primitive peridotite, PHN1611 (*7*), and the melt by partial melt-

Institute of Mineralogy, Petrology, and Economic Geology, Tohoku University, Sendai 980, Japan.

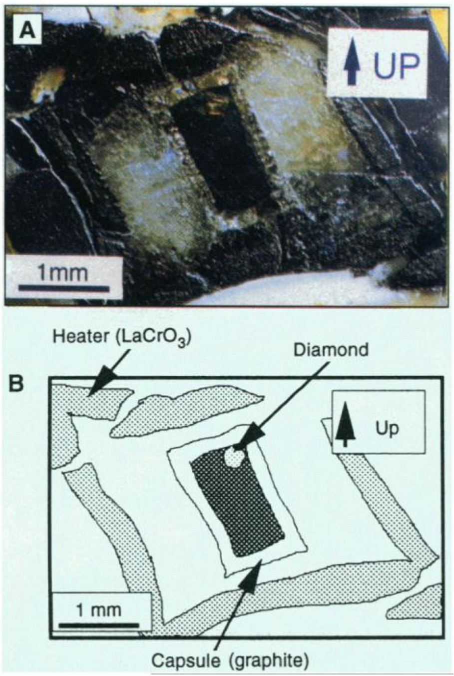

Fig. 1. (**A**) Photomicrograph and (**B**) sketch of the run product showing the flotation of diamond in the PHN1611 melt at 20.7 GPa and 2360°C.

Table 1. The experimental conditions and the results.

Run no.	P (GPa)	T (°C)	Time (min)	Result*
	PHN1611 composition†			
PHN-10	20.2	2360	5	S
PHN-12	20.7	2360	5	F
PHN-11	21.2	2360	5	F
PHN-08	22.1	2360	5	F
	IT8720 composition‡			
IT-04	14.0	2270	5	S
IT-07	14.9	2270	5	S
IT-09	15.8	2270	6	S
IT-06	16.7	2270	5	F
IT-08	16.7	2360	5	F
IT-03	19.2	2270	5.2	F

*S, sink; F, float. †The starting composition of PHN1611 was 45.1% (by weight) SiO_2, 2.8% Al_2O_3, 10.4% FeO, 38.4% MgO, and 3.4% CaO. Mg# = 100MgO/(MgO + FeO) (in mole percent) = 86.9 (*7, 9*). ‡The starting composition of IT8720 was 41.2% (by weight) SiO_2, 3.7% Al_2O_3, 15.1% FeO, 33.0% MgO, and 7.0% CaO. Mg# = 79.6 (*8, 9*).

ing of PHN1611 at 20 GPa (*8*), which we named IT8720. The starting materials were composed of olivine, orthopyroxene, clinopyroxene, and anorthite (*9*). A synthetic diamond single crystal with a diameter of around 400 μm was used as the buoy to measure the density of the peridotite melts at high pressure. We conducted experiments from 14.0 to 22.1 GPa at around 2300°C (*10*). Heating durations were about 5 min.

In a run quenched from 20.7 GPa (corresponding to the base of the transition zone) and 2360°C, diamond was less dense than the PHN1611 primitive mantle melt

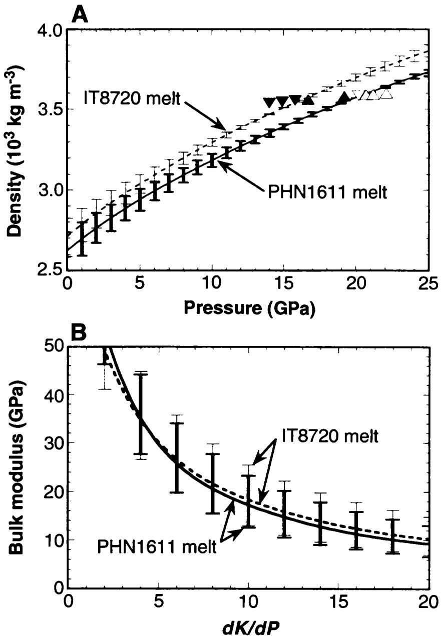

Fig. 2. (**A**) The experimental results on compression of the PHN1611 and IT8720 melts. Triangles and reversed triangles represent flotation and sinking of diamond, respectively (open symbols, PHN1611 melt; solid symbols, IT8720 melt). Diamond floats at high pressure in both melts. The density curves are expressed by the Birch-Murnaghan equation of state with a density $\rho_0 = 2620 \pm 120$ kg m^{-3} (*19*) and bulk modulus K = 36 ± 8 GPa, assuming a pressure derivative K' = 4 for PHN1611 melt at 2360°C, and $\rho_0 = 2710 \pm 120$ kg m^{-3} (*19*) and K = 36 ± 9 GPa, assuming K' = 4 for IT8720 melt at 2270°C. The parameters used for calculation of the density of the diamond marker are ρ_0(25°C) = 3515 kg m^{-3}, thermal expansion coefficient α(25°C) = 0.24 × 10^{-5} K^{-1}, temperature derivative $d\alpha/dT$ = 10^8 K^{-2}, K(25°C) = 442 GPa, dK/dT(25°C) = −0.0154 GPa K^{-1}, d^2K/dT^2 = −2.01 × 10^{-5} GPa K^{-2}, and K' = 4.03 (*20*). (**B**) The relation between the bulk modulus K and its pressure derivative K' for the PHN1611 and IT8720 melts.

(Fig. 1). The density crossover between the primitive mantle melt and diamond is at a pressure of 20.5 GPa at 2360°C, and the density of the melt at this point is 3590 ± 20 kg m^{-3} (Fig. 2A). The density crossover between diamond and the partial melt, the IT8720 melt, is at 16.3 GPa and 2270°C (Fig. 2A); the density of this melt here is 3560 ± 30 kg m^{-3}.

It is not possible to determine the density curve of the peridotite melts uniquely on the basis of the diamond flotation experiments, but we can estimate the possible relation between the bulk modulus K and its pressure derivative K' for the Birch-Murnaghan equation of state of the peridotite melts (Fig. 2B). Agee and Walker (*4*) estimated that the density crossover between peridotite melt and olivine is at around 11 GPa and 2000°C. Our measurements imply that the density crossovers between olivine and the PHN1611 melt at 2360°C and that between

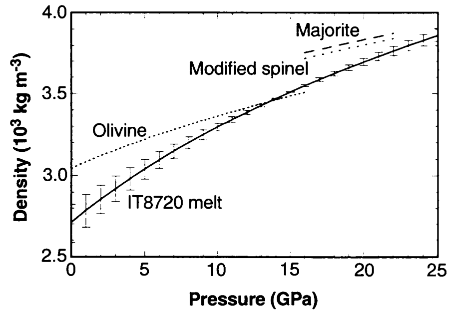

Fig. 3. The density relations between the IT8720 melt and coexisting phases, olivine, majorite, and modified spinel at 2270°C. Majorite and modified spinel are denser than the IT8720 melt at high pressure; that is, there is no density crossover in the transition zone.

the IT8720 melt and olivine at 2270°C may be at around 17 and 13 GPa, respectively, for K' = 4. For a greater K', the density crossover is at a lower pressure. Further, the pressure of the density crossover is reduced as temperature is decreased because of the large difference of the thermal expansion coefficients of olivine and the peridotite melt. As a result of the density crossover, olivine could accumulate in the upper mantle during solidification of a magma ocean (*2*), although viscosity of the melt and grain sizes of the crystals also control the nature of any stratification of the mantle (*11*). At ~20 GPa, majorite appears as the liquidus phase in a peridotite composition, and magnesiowustite and modified spinel coexist with the melt above the solidus (*12*). The compression curves indicate that the peridotite melts are less dense than these minerals (Fig. 3).

Diamond is transported to Earth's surface by kimberlite magmas, which are enriched in volatiles. The volatile-enriched compositions of kimberlite magmas may be a signature of shallower depths by assimilation of metasomatic horizons at the lithospheric metasome or at the lithosphere-asthenosphere boundary (*13*). In these models, the proto-kimberlite magma is a deeply derived ultramafic melt transported from the transition zone, and possibly from the lower mantle or the core-mantle boundary (*14*). Some diamonds contain high-pressure mineral inclusions such as majorite, (Mg,Fe)O, $CaSiO_3$, and (Mg,Fe) SiO_3; the latter two are assumed to have had perovskite structures. These minerals are consistent with derivation in the transition zone and the lower mantle (*15*). The spiral growth textures recorded on surfaces of some diamonds indicate growth from silicate melts (*16*). Our experiments imply that diamond crystals precipitated or trapped in silicate melts at the base of the transition zone and the lower mantle will tend to float and accumulate at a depth of 500 to 600 km in the early magma ocean stage or during the plume activities in the geological time. Thus, the transition zone could be a diamond-enrichment zone and, therefore, is a potential reservoir of diamond in Earth.

REFERENCES AND NOTES

1. E. Stolper *et al.*, *J. Geophys. Res.* **86**, 6261 (1981); E. G. Nisbet and D. Walker, *Earth Planet. Sci. Lett.* **60**, 105 (1982); E. Ohtani, *ibid.* **67**, 261 (1984)
2. E. Ohtani, *Phys. Earth Planet. Inter.* **38**, 70 (1985); C. B. Agee and D. Walker, *Earth Planet. Sci. Lett.* **90**, 144 (1988).
3. G. H. Miller, E. M. Stolper, T. J. Ahrens, *J. Geophys. Res.* **96**, 11831 (1991); E. Ohtani, A. Suzuki, T. Kato, *Proc. Jpn. Acad. Ser. B* **69**, 23 (1993).
4. C. B. Agee and D. Walker, *Earth Planet. Sci. Lett.* **114**, 315 (1993).
5. M. Kitamura, *Chikyu Monthly (Gekkan Chikyu)* **13**, 582 (1991) [in Japanese].
6. Pressure was calibrated on the basis of the α-β transition of Mg_2SiO_4 (*17*) and the ilmenite-perovskite transition of $MgSiO_3$ (*18*). We used a graphite capsule and a $LaCrO_3$ heater.
7. P. H. Nixon and F. R. Boyd, in *Lesotho Kimberlites*, P. H. Nixon, Ed. (Lesotho National Development, Maseru, South Africa, 1973), pp. 48–56.
8. E. Ito and E. Takahashi, *Nature* **328**, 514 (1987).
9. We synthesized the starting materials by heating stoichiometric mixtures of reagents for about 20 hours at 1000°C; the oxygen fugacity was controlled around the fayalite-magnetite-quartz (FMQ) buffer.
10. Temperature was estimated by the power versus temperature relation in separate runs (a W25%Re-W3%Re thermocouple was used for monitoring temperature). The errors in temperature are ±100°C.
11. W. B. Tonks and H. J. Melosh, in *Origin of the Earth*, H. E. Newsom and J. H. Jones, Eds. (Oxford Univ. Press, New York, 1990), pp. 151–174.
12. J. Zhang and C. Herzberg, *J. Geophys. Res.* **99**, 17729 (1994).
13. P. J. Wyllie, *ibid.* **85**, 6902 (1980); S. E. Haggerty, *Nature* **320**, 34 (1986).
14. S. T. Crough *et al.*, *Earth Planet. Sci. Lett.* **50**, 260 (1980); A. P. le Roex, *Nature* **324**, 243 (1986); S. E. Haggerty, *Earth Planet. Sci. Lett.* **122**, 57 (1994).
15. R. O. Moore and J. J. Gurney, *Nature* **318**, 553 (1985); R. S. Rickard *et al.*, *Geol. Soc. Aust. Spec. Publ.* **14**, 1054 (1989); B. Harte and J. W. Harris, *Mineral. Mag.* **58A**, 384 (1994).
16. I. Sunagawa, in *Material Science of the Earth's Interior*, I. Sunagawa, Ed. (TERRAPUB, Tokyo, 1984), pp. 303–330.
17. H. Morishima *et al.*, *Science* **265**, 1202 (1994).
18. H. Yusa *et al.*, *J. Geophys. Res.* **98**, 6453 (1993).
19. R. L. Lange and I. S. E. Carmichael, *Rev. Mineral.*, MSA short course volume, **24**, 25 (1990).
20. We calculated the isothermal compression curve of diamond from the following data sources: H. J. McSkimin and P. Andreatch, *J. Appl. Phys.* **43**, 2944 (1972); E. S. Zouboulis and M. Grimsditch, *High Pressure Res.* **9**, 218 (1992); S. K. Saxena, N. Chatterjee, Y. Fei, G. Shen, *Thermodynamic Data on Oxides and Silicates* (Springer-Verlag, Berlin, 1993).

21. We thank M. Kitamura and K. Onuma for discussion.

28 February 1995; accepted 18 May 1995

Age-Related Reductions in Human Recognition Memory Due to Impaired Encoding

Cheryl L. Grady,* Anthony R. McIntosh, Barry Horwitz, Jose Ma. Maisog, Leslie G. Ungerleider, Marc J. Mentis, Pietro Pietrini, Mark B. Schapiro, James V. Haxby

The participation of the medial temporal cortex and other cerebral structures in the memory impairment that accompanies aging was examined by means of positron emission tomography. Cerebral blood flow (rCBF) was measured during encoding and recognition of faces. Young people showed increased rCBF in the right hippocampus and the left prefrontal and temporal cortices during encoding and in the right prefrontal and parietal cortex during recognition. Old people showed no significant activation in areas activated during encoding in young people but did show right prefrontal activation during recognition. Age-related impairments of memory may be due to a failure to encode the stimuli adequately, which is reflected in the lack of cortical and hippocampal activation during encoding.

Lesion studies have shown that medial temporal areas, including the hippocampus and adjacent cortices, play a critical role in declarative, or explicit, memory, specifically in the encoding of new memories (*1*, *2*). In brain-damaged patients, the loss of medial temporal structures results in severe anterograde amnesia and in lesser degrees of retrograde amnesia (3). Lesions in animals also have shown memory performance to be dependent on both the hippocampus and adjacent structures (*4*). One theory (*1*) is that the hippocampus participates in the storage of new memories by binding together neural activities in distributed regions of the cortex, so that later presentation of all or part of the stimulus context can reactivate the entire network and facilitate retrieval. The role of the hippocampus is thought to be limited in time, so that at some point after the new memory is processed, it can be retrieved without hippocampal involvement (*5*). Other regions also participate in memory, such as the prefrontal cortex (*6–8*), which shows frequency potentiation, similar to that seen in the hippocampus, during conditioning (9), and the inferior temporal cortex (*10*), which interacts with the prefrontal cortex during encoding of visual associative (*11*) and delayed match-to-sample tasks (*7*) in monkeys.

The degree of memory impairment with aging varies; explicit memory is reduced in old compared with young people, but little change is seen in implicit memory (*12*). There are changes in the hippocampus with aging, including reductions in long-term potentiation (*13*), loss of afferent input (*14*), and loss of neurons (*15*). Some age-related hippocampal changes such as increased dendritic arborization may be a compensatory response to loss of cells or input (*16*). There also are age-related changes in other areas of the cortex, such as reductions in neurons (*17*), dendrites (*18*), and synapses, particularly in the frontal cortex (*19*). However, the relation between these changes and age-related reductions in human memory is unknown.

In a previous experiment (*20*), we used positron emission tomography (PET) to measure regional cerebral blood flow (rCBF) in young people during encoding and recognition of faces. The medial temporal cortex, including the hippocampus, showed increased rCBF (rCBF activation) during encoding of new memories but not during recognition. The prefrontal cortex was activated during both conditions: in the left hemisphere during encoding and in the right hemisphere during recognition. Here we discuss young and old people (Table 1) who underwent repeated PET scans (*21*) while performing three tasks twice in the following order: memorizing a set of faces (encoding), face matching (perception), and face recognition. A sensorimotor control task also was performed at the beginning and end of each scanning session. During the encoding task, subjects were shown 32 unfamiliar faces and asked to memorize them. Each face was shown for 4 s, and the entire set was shown three times, in a different order each time. The matching task used different faces from the memorization set and was a forced-choice match-to-sample task in which the sample face and two

C. L. Grady, A. R. McIntosh, B. Horwitz, M. J. Mentis, P. Pietrini, M. B. Schapiro, Brain Aging and Dementia Section, Laboratory of Neuroscience, National Institute on Aging, National Institutes of Health (NIH), Building 10, Room 6C414, 9000 Rockville Pike, Bethesda, MD 20892, USA.
J. M. Maisog and J. V. Haxby, Section on Functional Brain Imaging, Laboratory of Psychology and Psychopathology, National Institute of Mental Health, NIH, Building 10, Room 4C110, 9000 Rockville Pike, Bethesda, MD 20892, USA.
L. G. Ungerleider, Section on Neurocircuitry, Laboratory of Neuropsychology, National Institute of Mental Health, NIH, Building 49, Room 1A75, 9000 Rockville Pike, Bethesda, MD 20892, USA.

*To whom correspondence should be addressed.